© 2018. Published by The Company of Biologists Ltd | Journal of Cell Science (2018) 131, jcs216556. doi:10.1242/jcs.216556

RESEARCH ARTICLE

Switch-like PKA responses in the nucleus of striatal neurons

Cédric Yapo[1], Anu G. Nair[2,3,4,‡], Jeanette Hellgren Kotaleski[2,5], Pierre Vincent[1,*,§] and Liliana R. V. Castro[1,*]

ABSTRACT

Although it is known that protein kinase A (PKA) in the nucleus regulates gene expression, the specificities of nuclear PKA signaling remain poorly understood. Here, we combined computational modeling and live-cell imaging of PKA-dependent phosphorylation in mouse brain slices to investigate how transient dopamine signals are translated into nuclear PKA activity in cortical pyramidal neurons and striatal medium spiny neurons. We observed that the nuclear PKA signal in striatal neurons featured an ultrasensitive responsiveness, associated with fast all-or-none responses, which is not consistent with the commonly accepted theory of a slow and passive diffusion of catalytic PKA in the nucleus. Our numerical model suggests that a positive feed-forward mechanism inhibiting nuclear phosphatase activity – possibly mediated by DARPP-32 (also known as PPP1R1B) – could be responsible for this non-linear pattern of nuclear PKA response, allowing for a better detection of the transient dopamine signals that are often associated with reward-mediated learning.

KEY WORDS: Protein kinase A, Biosensor imaging, Modeling, Nucleus, Signal integration

INTRODUCTION

The cAMP–PKA signaling pathway plays a key role in virtually all cell types by acutely regulating various cell functions, such as metabolism, motility and excitability. This signaling cascade additionally exerts long-term effects by regulating the expression of genes in the nucleus. Despite considerable knowledge obtained through decades of studies on PKA signaling, its dynamics in the nucleus remains poorly characterized. The PKA holoenzyme is a tetramer comprising two catalytic (C) and two regulatory (R) subunits, for which several isoforms have been described: three catalytic isoforms (Cα, Cβ and Cγ, encoded by *PRKACA*, *PRKACB* and *PRKACG*, respectively) can bind to four different R isoforms (RIα, RIβ, RIIα and RIIβ, encoded by *PRKAR1A*, *PRKAR1B*, *PRKAR2A* and *PRKAR2B*, respectively). RIIβ is the most abundant regulatory subunit in many types of neurons (Cadd and McKnight, 1989), and is required for the nuclear integration of PKA signals (Brandon et al., 1998). In the case of the type II PKA holoenzyme, an increase in cAMP concentration releases the catalytic subunits, which can then diffuse throughout the cell (Kim et al., 2011; Martin et al., 2007; Tillo et al., 2017), and the passive diffusion of the catalytic subunit through the nuclear pore is thought to be the main mechanism whereby the cAMP–PKA signal is transduced into the nucleus. Experiments performed with chemically labeled PKA subunits have shown that this diffusion process occurred on a time scale of tens of minutes, and is associated with CREB phosphorylation and the induction of gene expression (Hagiwara et al., 1993; Harootunian et al., 1993; Meinkoth et al., 1990). Although neurons in several brain regions seem to follow this signaling scheme (Gervasi et al., 2007; Hu et al., 2011), it remains puzzling that a specific brain region, the striatum, responds with superior sensitivity to dopamine signals: addictive drugs for instance, which trigger a large release of dopamine in the cortex and the striatum, increase the expression of c-Fos primarily in the striatum through the activation of D_1 receptors (Graybiel et al., 1990; Harlan and Garcia, 1998).

Dopamine is released in the striatum and prefrontal cortex by the midbrain dopaminergic neurons. The effects of dopamine are mediated by the D_1-like (DRD1, DRD5) and D_2-like (DRD2, DRD3, DRD4) receptors, which oppositely modulate the cAMP–PKA signaling pathway, thereby regulating a number of neuronal properties (Beaulieu et al., 2015; Girault, 2012; Threlfell and West, 2013; Tritsch and Sabatini, 2012). In the dorsal striatum, these receptors are expressed on two different types of medium-sized spiny neurons (MSNs), hereafter called D1 and D2 MSNs (Le Moine and Bloch, 1995; Valjent et al., 2009). Transient dopamine stimulations trigger opposite changes in cAMP–PKA signaling in these neurons, over a time-scale of a few minutes, which can be recorded through biosensor imaging (Yapo et al., 2017). The burst firing of dopaminergic neurons leads to the phasic release of dopamine, and supports a wide range of functions associated with salience and reward processing (Arbuthnott and Wickens, 2007; Bromberg-Martin et al., 2010; Schultz, 2007). Despite the briefness of phasic dopamine release, burst firing of the dopamine neurons triggers the induction of immediate early genes (IEGs) in D1 MSNs, leading to long-term changes in gene expression and plasticity in the striatal neurons (Chergui et al., 1996; Howard et al., 2013). Striatal neurons differ from cortical neurons notably because they have a higher expression level of dopamine receptors or DARPP-32 (also known as PPP1R1B), and express specific signaling proteins such as $G_{\alpha olf}$, type V adenylyl cyclase and type 10 phosphodiesterase. These unusual signaling enzymes are associated with faster and larger cAMP–PKA responses to dopamine in the cytosol (Castro et al., 2013), and we wanted to explore whether signal transduction in the nucleus of striatal neurons also possessed specific mechanisms to enhance its sensitivity. To answer this question, we combined live-cell imaging of PKA activity in the cytosol and nucleus, with computational modeling based on our previously published model (Yapo et al., 2017). We found that transient dopamine stimuli trigger ultrasensitive and switch-like nuclear PKA responses in the striatum, and our computer model suggests that this feature depends on a

[1]Sorbonne Université, CNRS, Biological Adaptation and Ageing, F-75005 Paris, France. [2]Science for Life Laboratory, School of Computer Science and Communication, KTH Royal Institute of Technology, Stockholm, 10044, Sweden. [3]National Centre for Biological Sciences, Tata Institute of Fundamental Research, Bangalore 560065, India. [4]Manipal University, Manipal 576104, India. [5]Department of Neuroscience, Karolinska Institutet, Solna, 17177, Sweden.
‡Present address: Institute of Molecular Life Sciences, University of Zurich, Winterthurerstrasse 190, 8057 Zurich, Switzerland.
*These authors contributed equally to this work

§Author for correspondence (pierre.vincent@upmc.fr)

A.G.N., 0000-0002-1952-9583; J.H.K., 0000-0002-0550-0739; P.V., 0000-0002-8479-1908; L.R.V.C., 0000-0001-8902-089X

Received 6 February 2018; Accepted 25 June 2018

Journal of Cell Science (2018) 131, jcs216556. doi:10.1242/jcs.216556

positive feed-forward mechanism in the nucleus, which results in a high PKA to protein phosphatase activity ratio.

RESULTS

Transient dopamine stimulations lead to robust and fast PKA signaling in the nucleus of D1 MSNs

We first tested whether a transient dopamine stimulus was sufficient to trigger a PKA-dependent response in the nucleus. Dopamine D_1 receptors in striatal and cortical neurons (layer V) were briefly stimulated by dopamine released from NPEC-DA (5 µM) by means of a flash of UV light (0.1 or 1 s duration). We monitored the induction of c-Fos, an IEG induced by dopamine (Chergui et al., 1996). Nuclei positive for c-Fos expression were counted, and a robust increase in c-Fos expression was observed in the striatum 1.5 h following dopamine uncaging (Fig. 1A). The same protocol applied to the prefrontal cortex elicited no response (Fig. 1B). As a positive control, brain slices treated for 5 min with the adenylate cyclase activator forskolin (fsk, 13 µM) showed increased c-Fos immunoreactivity in both striatum and cortex. This suggests that, unlike cortical neurons, striatal MSNs efficiently transduce a transient neuromodulatory signal in the nuclear compartment.

We then monitored the dynamics of PKA signaling in the cytosolic and nuclear compartments using the AKAR3 and AKAR2-NLS biosensors, respectively (Allen and Zhang, 2006; Zhang et al., 2005). Both biosensors report changes in the PKA-to-phosphatase equilibrium through a change in FRET efficacy, which was quantified with wide-field ratiometric imaging. Dopamine uncaging in the striatum (UV 0.1 s) rapidly increased the AKAR2-NLS signal ratio in D1 MSNs (Fig. 1C). After recovery of the ratio, application of a saturating dose of the D_1-like receptors agonist SKF-38393 (SKF, 1 µM) triggered a steep elevation of the biosensor response, which was not further increased by the application of adenylyl cyclase activator forskolin (fsk, 13 µM). This same protocol of 0.1 s uncaging produced no response in the nucleus of cortical neurons, and we increased the UV duration (1 s instead of 0.1 s) to release more dopamine: yet, cortical neurons remained unresponsive (Fig. 1D). Subsequent stimulation of the D_1 receptors with SKF eventually induced a large, but submaximal, increase in the AKAR2-NLS ratio, a response which appeared to have slower kinetics compared to the SKF response in D1 MSNs. Overall, 77±13% (results in main text are mean±s.e.m.) of the neurons in layer V of the prefrontal cortex responded positively to D_1 receptor stimulation with 1 µM SKF at the cytosolic level [n=172; N=11; where 'N' indicates the number of independent experiments (i.e. brain slices), and 'n' indicates the number of cells]. Similar experiments were repeated and averaged using either the AKAR3 or AKAR2-NLS biosensors; although the cytosolic signals were of similar amplitude in striatal and cortical neurons, only striatal neurons displayed a nuclear response (Fig. 1E,F).

To ensure that the measurements were comparable between the two brain regions, we tested whether the dynamic range of the AKAR2-NLS biosensor was the same in the striatum and in the cortex. The maximal ratio change was taken as the $\Delta R/R$ value between the basal ratio and the highest ratio response obtained in the experiment (1 µM SKF or 13 µM fsk). This value showed no difference (11.18±0.12, n=271, N=19 in the cortex versus 11.20±0.23, n=217, N=26 in the striatum; P=0.9, unpaired t-test), indicating that the biosensor reports changes in PKA-to-phosphatase equilibrium in a same dynamic range in both brain regions.

Cortical neurons express D_1- as well as D_2-like receptors, which exert antagonistic effects on PKA signaling (Beaulieu et al., 2015; Vincent et al., 1993). To rule out interactions with D_2 receptors, we replaced dopamine uncaging with applications of the D_1-like agonist SKF-38393 (SKF, 1 µM). SKF was applied briefly (10 s) with a fast microperfusion system, then the drug was washed-out in the bath perfusion. The cytosolic or nuclear PKA signals were monitored with the biosensors AKAR3 and AKAR2-NLS, respectively. Similar to what was observed with dopamine uncaging, the 10 s SKF stimulation failed to induce any AKAR2-NLS response in the cortex, whereas D1 MSNs in the striatum still displayed a robust response (Fig. 2A,B). We then tested the effect of sustained D_1 receptor stimulation on both cortical and striatal neurons. SKF (1 µM) was applied using the fast microperfusion system, and its application on the slice was maintained until a steady-state response was reached (Fig. 2C,D). The maximal response in cytosolic PKA signal was reached in less than 1 min in both striatum and cortex, with the striatum response being faster than that from the cortex, as expected from our previous work (Castro et al., 2013). In contrast to the rapid PKA activation seen in the cytosol, the nuclear PKA signal proceeded at a slower pace in both cell types [time to the half-maximum response ($t_{1/2on}$) 482±22 s, N=5 in the cortex versus 211±6 s, N=6 in the striatum], with the nuclear response in the striatum remaining faster and of larger amplitude than in the cortex (Fig. 2C,D). Similarly fast nuclear kinetics were also observed in D2 MSNs following stimulation of the adenosine A_{2A} receptors with CGS21680 (Fig. 2E), showing that the fast responsiveness is a shared feature of both subtypes of striatal MSNs.

Striatal neurons express high densities of dopamine receptors and G proteins. Therefore, we wondered whether the fast responsiveness resulted from this or from other downstream mechanisms. In order to bypass the first level of signal integration, we directly stimulated adenylyl cyclases with forskolin, and to take out of the equation the degradation pathway, phosphodiesterases were blocked with IBMX. Rapid application of fsk+IBMX produced nuclear responses that were faster in the striatum than in the cortex ($t_{1/2on}$=399±13 s, N=7 in the cortex versus 249±9, N=6 in the striatum, unpaired two-tailed Student's t-test, P<0.05; Fig. 2F) showing that, indeed, striatal neurons possess specific mechanisms downstream of the receptor that speed-up nuclear integration of PKA signals.

Switch-like nuclear PKA responses in the striatum

The efficiency of transient dopamine signals in inducing a nuclear response, as well as its speed depicted above, suggested some non-linear effect in signal integration in MSNs, which could affect the responsiveness to low doses of SKF. We used the fast perfusion system to perform sustained SKF stimulations at low doses, ranging from 0.1 to 10 nM, and we measured the amplitude of the SKF-induced nuclear response using AKAR2-NLS, again comparing striatum and cortex. A single low dose of SKF was tested in each experiment. At the end of the recording, 1 µM SKF was applied to reveal D1 MSNs. This level was used as maximum for normalization, as the application of fsk at the end of the recording produced no further increase. At a concentration of 2 nM SKF for instance (Fig. 3A, left), D1 MSNs showed either no or very small responses, or an almost maximal response. In contrast, cortical neurons stimulated with 10 nM SKF responded with a continuum of amplitudes (Fig. 3A, right). At the end of the recording, 1 µM SKF was applied to reveal the cortical neurons which express D_1 receptors (estimated to be 77%, see above). Further application of fsk at the end of the recording increased the ratio to the value considered as maximal, and was used for normalization.

The same type of experiment was repeated using different concentrations of SKF for the first stimulation, and the amplitude of

Journal of Cell Science (2018) 131, jcs216556. doi:10.1242/jcs.216556

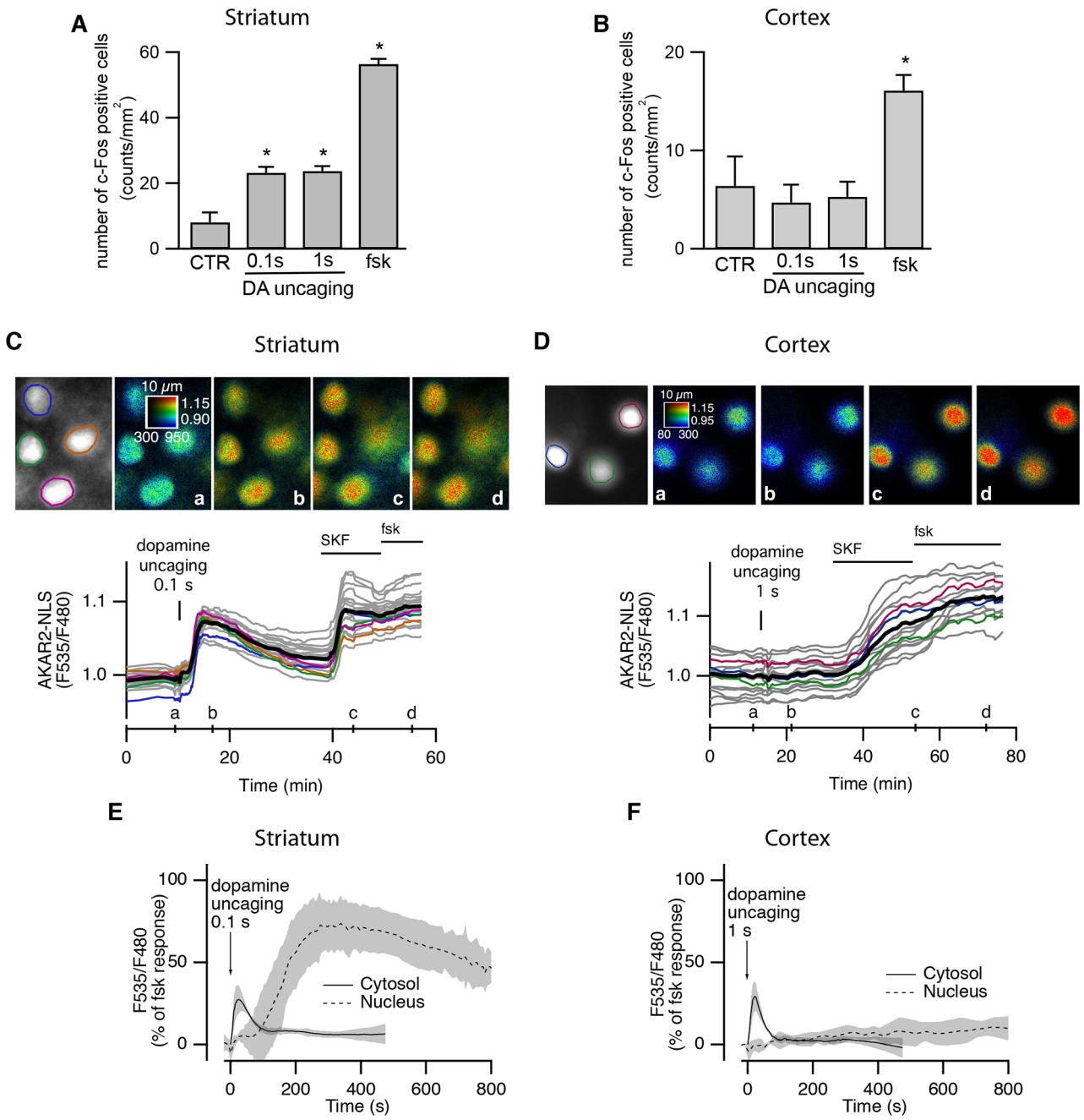

Fig. 1. A brief dopamine stimulation triggers a nuclear PKA signal in the striatum but not in the prefrontal cortex. (A,B) c-Fos-positive nuclei in the dorsal striatum (A) and prefrontal cortex (B) following dopamine uncaging (5 µM NPEC-DA, uncaging for 0.1 s and 1 s) or application of the adenylyl cyclase activator forskolin (fsk, 13 µM, applied for 5 min). (C,D) Wide-field imaging of the AKAR2-NLS sensor in the dorsal striatum (C) and prefrontal cortex (D). Raw fluorescence of the donor is displayed in gray and the donor:acceptor fluorescence ratio is displayed in pseudo-color. Each trace on the graph indicates the F535/F480 emission ratio measurement on regions indicated by the color contour drawn on the gray image. Traces in gray correspond to nuclei outside this region of the image. The thick black traces represent averages. Ratio images (a–d) correspond to the time points indicated in the bottom graph. Dopamine released from NPEC-DA (5 µM, 0.1 s or 1 s) by UV uncaging generates a transient positive response in medium-sized spiny neurons of the striatum (C) but not in the cortex (D). The D_1 receptor agonist SKF-38393 (SKF, 1 µM) and forskolin (fsk, 13 µM) are applied at the end of the experiment as positive controls. (E,F) The traces of individual cells and their average ratio responses are normalized with respect to the maximal fsk response. PKA signals in the cytosol and nucleus are measured with AKAR3 and AKAR2-NLS biosensors, respectively. The line represents the mean, the gray shade represents s.e.m.

this SKF response was plotted for each individual neuron against SKF concentration (Fig. 3B). In the striatum, as SKF concentration increases, more cells exhibit a ratio change close to the maximum, while very few show an intermediate signal (Fig. 3B, left). In contrast, cortical neurons showed responses covering the whole range of amplitude level (Fig. 3B, right). For the highest dose (1 µM SKF), the response was smaller on average than for 100 nM, possibly because of desensitization of the D_1 receptor over long applications of high doses. Data were plotted as cumulative probabilities for each concentration, and showed a non-linear profile for the striatum (particularly visible for 1 nM SKF concentration), indicative of a bimodal distribution (Fig. 3C, left). Cumulative probabilities calculated for cortical neurons showed linear profiles for all concentrations (Fig. 3C, right). The pooled

Journal of Cell Science

Journal of Cell Science (2018) 131, jcs216556. doi:10.1242/jcs.216556

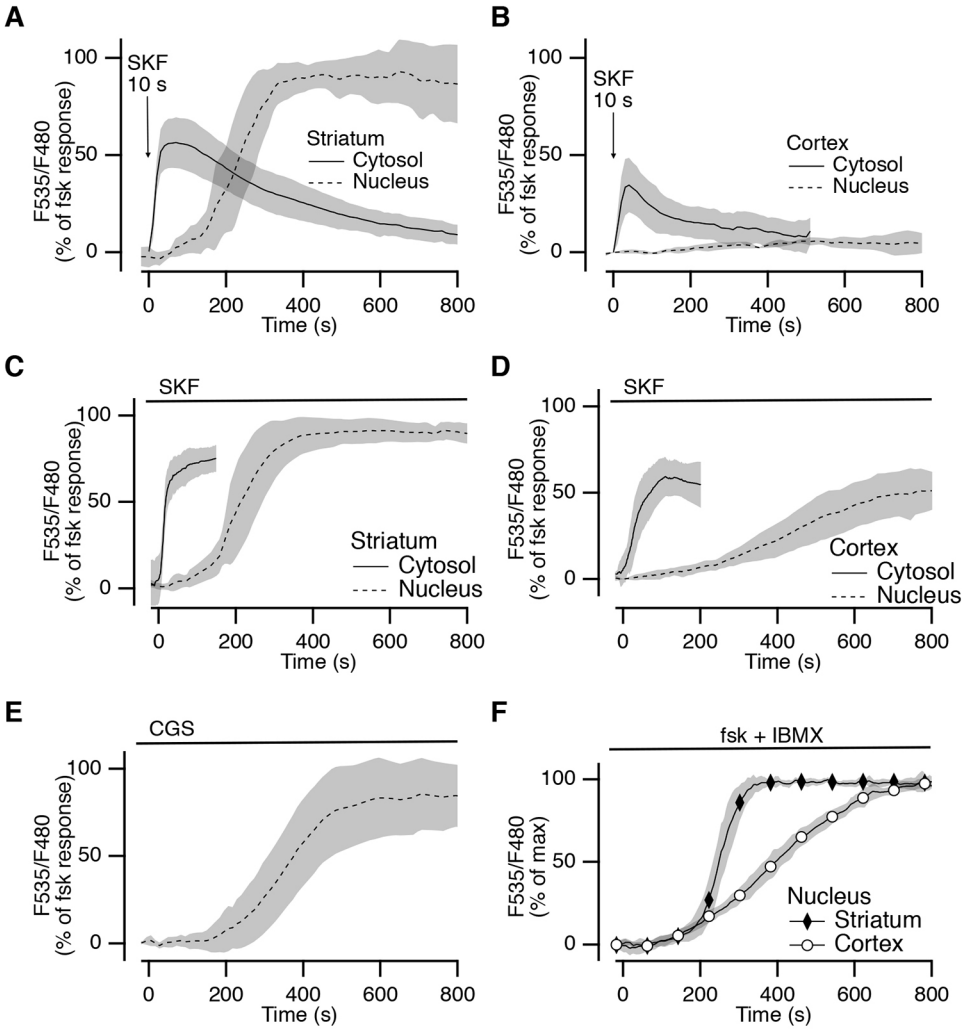

Fig. 2. Robust and fast PKA signal in the nucleus of striatal neurons. (A,B) Cytosolic (solid lines, measured with AKAR3) and nuclear (dotted lines, measured with AKAR2-NLS) PKA responses elicited by a 10 s application of the D_1-like agonist SKF-38393 (SKF, 10 s, 1 µM) in the striatum (A) and prefrontal cortex (B). (C,D) Onset of the cytosolic (solid lines) and nuclear (dotted lines) PKA responses in D1 MSNs (C) and cortical neurons (D) following sustained application of SKF. (E) Onset of the nuclear PKA response in D2 MSNs of the striatum following application of the A_{2A} agonist CGS 21680 (1 µM). (F) Onset of the nuclear PKA responses in D1 MSNs of the striatum and cortical neurons following sustained application of adenylyl cyclase activator forskolin (fsk, 13 µM) and the phosphodiesterase inhibitor IBMX (200 µM). Mean responses from four to six independent experiments/condition are represented and expressed as a percentage of the response to fsk or fsk+IBMX, as indicated. The shaded area represents the s.e.m.

responses of all individual striatal neurons (N=34, n=286) displayed as probability density graph showed a large peak at the maximal level that was separated from the baseline peak by a wide gap, a signature of an 'all-or-none' signal integration (Fig. 3D). This bimodal distribution contrasted with the graded responses measured in the prefrontal cortex (N=22, n=315), which showed a wide central peak that was not well separated from the baseline peak (Fig. 3D).

Overall, these results depict the nuclear compartment of MSNs as particularly responsive to transient stimulation of the D_1 receptors, producing robust PKA-dependent phosphorylations in both cytosolic and nuclear compartments, with a switch-like mechanisms that controls the transfer of the signal from the cytosol into the nucleus.

The nuclear responsiveness in D1 MSNs does not result from the existence of a nuclear pool of PKA

cAMP can diffuse freely throughout the cell and in the nucleus (DiPilato et al., 2004; Haj Slimane et al., 2014; Yang et al., 2014) and other studies have reported the presence of PKA holoenzyme in the nuclear compartment, which might support the fast kinetics of the nuclear PKA responses (Ilouz et al., 2017; Sample et al., 2012; Zippin et al., 2004). We tested this hypothesis in our preparations by photo-releasing cAMP inside the neurons using a cell-permeant caged cAMP (4,5-dimethoxy-2-nitrobenzyl adenosine 3,5-cyclic monophosphate, DMNB-cAMP). Striatal and cortical brain slices were incubated with DMNB-cAMP (10 µM) for 10 min, and wide-field uncaging with a 1 s UV flash was performed to increase cAMP levels evenly in all cellular compartments, including the nucleus. This type of stimulation induced a very fast and transient activation of PKA in the cytosol of both striatal and cortical neurons (Fig. 4). The amplitude of the transient cytosolic PKA responses reached ∼80% of maximal fsk-induced response in both cell types. However, in the nucleus, the PKA responses differed markedly: no response was observed in the cortex, whereas in the striatum, cAMP uncaging induced a robust increase in AKAR2-NLS ratio, with onset kinetics similar to that obtained with dopamine uncaging or upon a 10 s SKF stimulation. This further confirms that a same cAMP signal is integrated much more efficiently in striatal than in cortical neurons. More importantly, while AKAR3 instantly responded in the cytosol, a delay of ∼100 s was observed for the AKAR2-NLS response in striatal cells, which contradicts the hypothesis of PKA residing in the nucleus and being activated there, as the nuclear response would be expected to have the same kinetics as the cytosolic response if that were the case. Based on these results, we conclude that the AKAR2-NLS responses triggered by receptor stimulation or cAMP photorelease requires diffusion of PKA catalytic subunits into the nucleus.

PP1 activity reverts nuclear PKA signaling in the cortex

We then investigated the cellular mechanisms that dampen the cAMP–PKA signaling pathway in cortical neurons and may thus prevent the nuclear transduction of dopamine signals. Among these,

Journal of Cell Science (2018) 131, jcs216556. doi:10.1242/jcs.216556

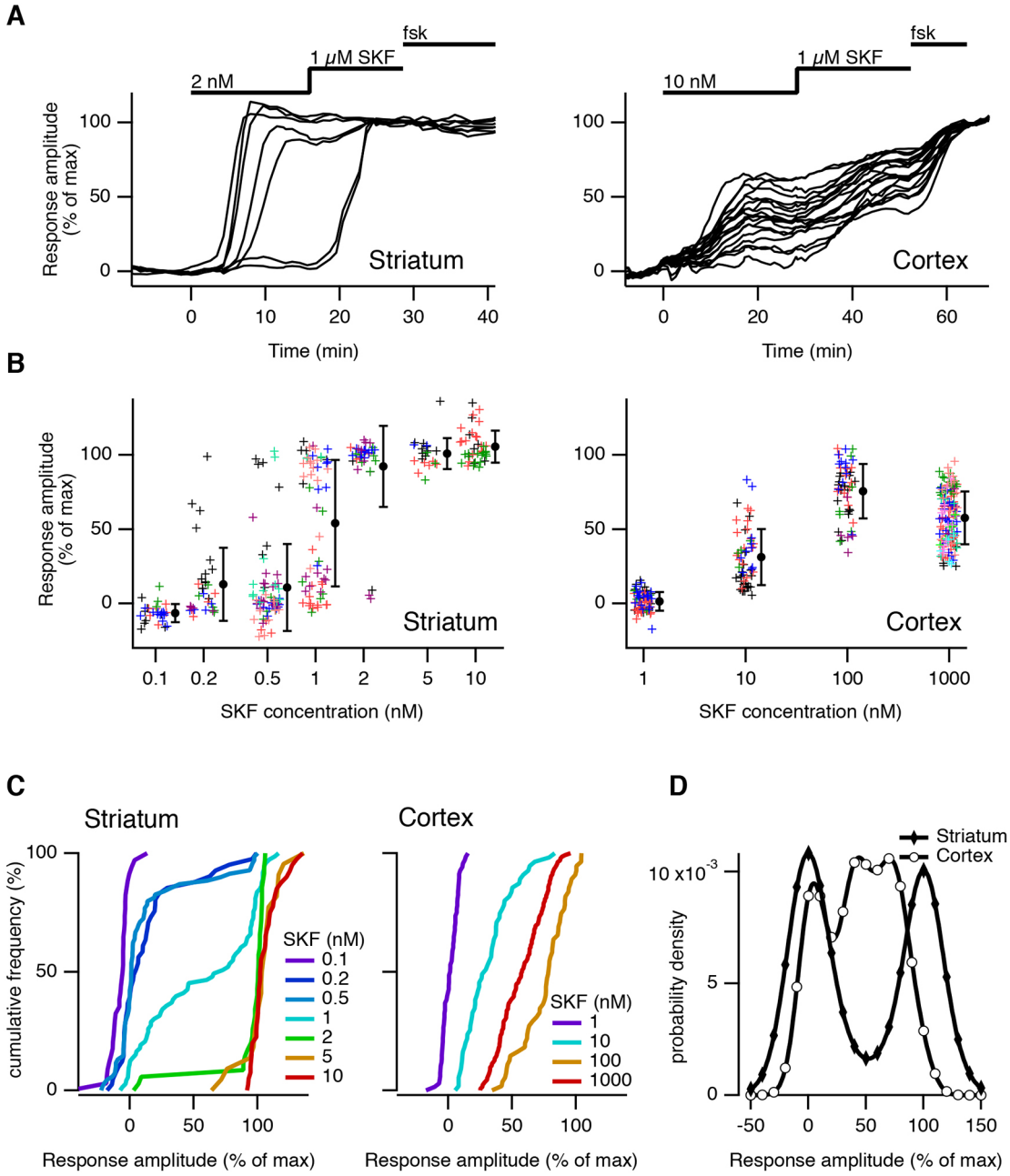

Fig. 3. Switch-like PKA responses in the nucleus of striatal neurons. (A) AKAR2-NLS normalized ratio during sustained application of the D_1-like agonist SKF-38393 (SKF). Two representative experiments in striatal (left) and cortical (right) brain slices are shown: each trace indicates the ratio measured on the nucleus of individual neurons, normalized between the basal and maximal ratio. The bars on top of the graph indicate the application of drugs. (B) Similar experiments were repeated with different doses of SKF for the first SKF application in the striatum (left) and in the cortex (right). Each neuron is represented by a marker on the graph. Neurons from the same experiment are displayed in the same color. The mean±s.e.m is indicated for each dose. (C) Same data as in B represented as cumulative frequencies for the striatum (left) and the cortex (right). Note the kink on the profile corresponding to 1 nM SKF in the striatum. (D) Probability density estimate of all pooled responses in the striatum and in the cortex.

it is known that the phosphodiesterase PDE4 powerfully controls cAMP levels in cortical neurons (Zhang et al., 2002) and we tested whether inhibiting PDE4 might reveal a nuclear response. As expected from our previous work (Castro et al., 2010, 2013), application of the PDE4 inhibitor rolipram (100 nM) increased the amplitude of the cytosolic AKAR3 response to a brief (10 s) SKF stimulation (Fig. 5A,B). However, even under PDE4 inhibition, the nucleus of cortical neurons barely responded to 10 s SKF stimulations (amplitude of the response at 800 s=4.4±2.2%, N=4 in control versus 19.6±5.5%, N=5 under rolipram, unpaired two-tailed t-test, P<0.05; Fig. 5C,D). These results indicate that in cortical neurons, although PDE4 activity affects the amplitude of the cytosolic PKA response, its effect in the nucleus is minimal, indicating that another mechanism is counteracting the nuclear PKA signal.

The phosphorylation level of PKA targets (including AKAR biosensors) proceeds from a balance between PKA and protein phosphatase activities; therefore, we hypothesized that higher protein phosphatase activities in cortical neurons might explain the lack of nuclear response. In the brain, PP1, PP2A and PP2B are

Journal of Cell Science (2018) 131, jcs216556. doi:10.1242/jcs.216556

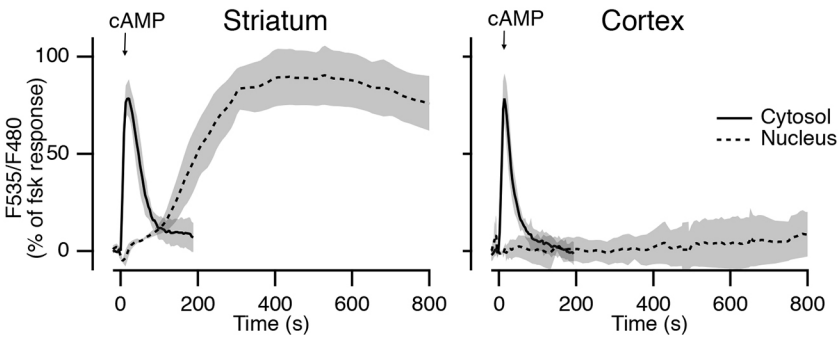

Fig. 4. Global cAMP uncaging produces a delayed PKA response in the nucleus of striatal neurons. Mean cytosolic (solid lines, measured with AKAR3) and nuclear (dotted lines, measured with AKAR2-NLS) PKA responses elicited by 1 s UV uncaging of cAMP from DMNB-cAMP (10 µM) in the striatum (left) and in the prefrontal cortex (right). Mean responses are expressed as the percentage of the maximal response to the adenylyl cyclase activator forskolin (fsk), and represent the average response from at least three independent experiments per condition. The shaded area represents the s.e.m.

the major serine/threonine protein phosphatases counteracting PKA effects. We had already reported that protein phosphatase inhibition with cantharidin efficiently prevented the dephosphorylation of AKAR in thalamic intralaminar neurons (Gervasi et al., 2007). In addition, in the striatum, cantharidin efficiently blocks the inhibitory effect of PP1 on the AKAR phosphorylation level (Polito et al., 2015). Here, in the prefrontal cortex, brief (10 s) SKF application in the presence of the non-selective PP1/PP2A inhibitor cantharidin (30 µM) produced a maximal increase in the nuclear PKA signal that did not return to the baseline following washout of SKF (Fig. 5E). Fostriecin (200 nM), a specific inhibitor of PP2A (Swingle et al., 2009), had very little effect on the nuclear response to brief SKF stimulation compared to cantharidin [Fig. 5F; amplitude of the response at 800 s=0.04±0.02%, N=4 in control versus 84.78±6.88%, N=5 under cantharidin versus 0.18±0.07, N=6 under fostriecin, expressed as % of maximal fsk response; one-way ANOVA: $F(2,12)=45.37$, $P<0.001$, followed by Bonferroni post hoc test]. These data show that protein phosphatase activities, and most likely that of PP1, strongly counterbalance nuclear PKA activity in cortical neurons and prevent transient cAMP signals from being integrated into a nuclear signal.

Computer modeling indicates the critical role played by the balance of PKA and protein phosphatase activities

Computer simulations were then used to analyze how striatal and cortical neurons differed in their integration of a PKA signal. To this

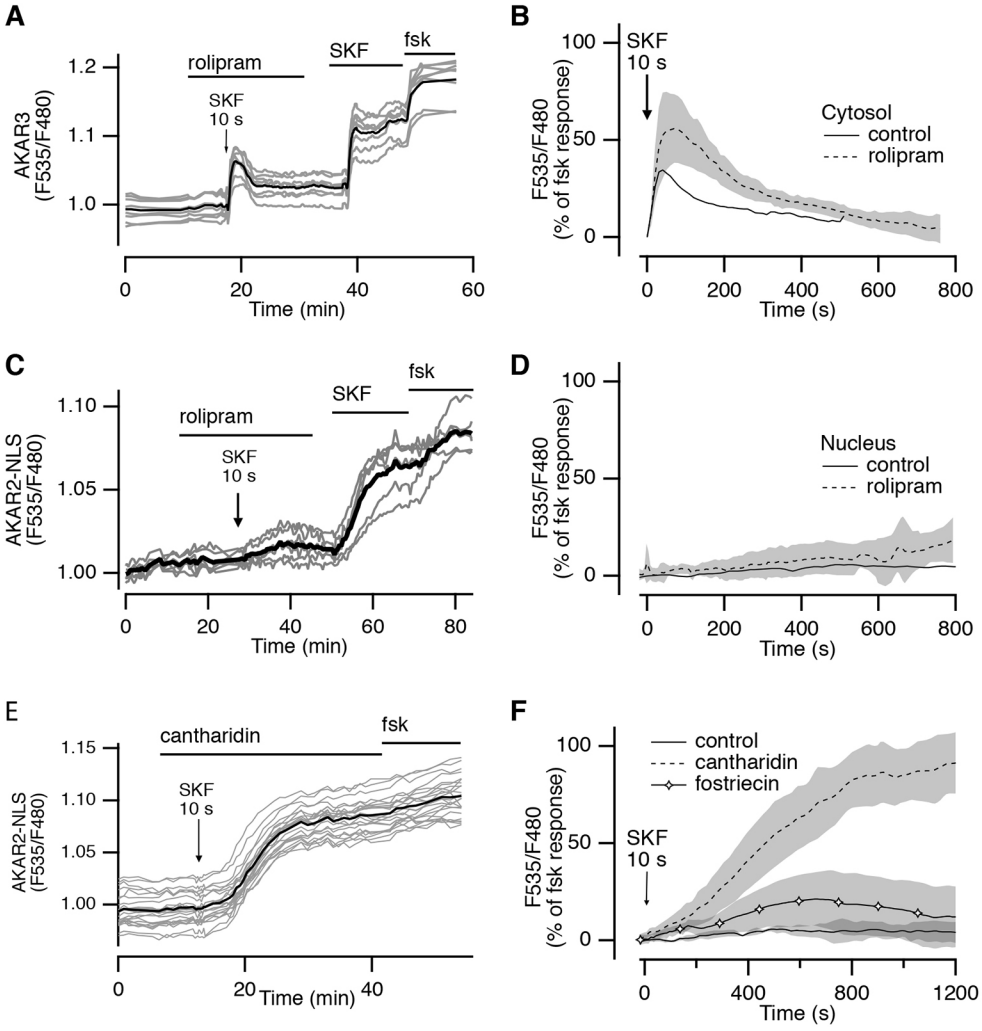

Fig. 5. Phosphatase activity prevents nuclear PKA signaling in the cortex. (A) PKA signal in the cytosol measured with AKAR3 sensor during the 10 s application of SKF (1 µM), in the presence of the PDE4 inhibitor rolipram (100 nM) in the prefrontal cortex. SKF and fsk (13 µM) were applied (sustained application) at the end of the experiment. (B) Means of same experiments performed with or without rolipram. (C) Same as A except that the PKA signal is measured in the nucleus with AKAR2-NLS. (D) Means of same experiments performed with or without rolipram. (E) Nuclear PKA responses elicited by a 10 s SKF application in the presence of the phosphatase PP1/PP2A inhibitor cantharidin (30 µM). Fsk was applied at the end of the experiment to elicit a maximal increase in the ratio change. (F) Averaged responses of the PKA signal to 10 s SKF alone, in the presence of cantharidin or fostriecin (PP2A inhibitor, 0.2 µM). Average responses are expressed as a percentage of the fsk response, and represent the mean response from at least four independent experiments per condition. The shaded areas represents the s.e.m.

Journal of Cell Science (2018) 131, jcs216556. doi:10.1242/jcs.216556

end, we used the experimentally constrained, mass-action kinetics model of cytosolic D_1-dependent cAMP–PKA signaling in striatal MSNs with all its parameters (Yapo et al., 2017) and extended it to the nucleus: this extension included the cyto-nuclear translocation of the catalytic subunit of PKA that phosphorylates nuclear AKAR, which is dephosphorylated by protein phosphatases (Fig. 6A).

The cyto-nuclear translocation of PKA is dictated by passive diffusion (Hagiwara et al., 1993; Harootunian et al., 1993), which was modeled as a first-order reversible reaction with fixed reaction rates (or static translocation rate). Simulating this static translocation rate for cyto-nuclear PKA translocation (Fig. 6A) with transient dopamine input (see Materials and Methods) produced a nuclear AKAR phosphorylation that had a nearly exponential onset kinetics (Fig. 6B, black trace). This onset kinetics was observed in several cell types (Harootunian et al., 1993; Yang et al., 2014) but not in striatal and cortical neurons, which displayed a sigmoidal response onset (Fig. 2). This suggests that PKA cyto-nuclear translocation in neurons involves an additional mechanism that introduces nonlinearity, such as a dynamic translocation rate (Fig. 6B); in this reaction scheme, PKA positively regulates its own translocation rate by changing the state of the nuclear pore via phosphorylation (Fig. 6B, inset). This is consistent with the previously reported increase in cyto-nuclear translocation mediated by PKA (Mishra and Parnaik, 1995). A similar observation was also made previously with respect to the extracellular signal-regulated kinases 1 and 2 (ERK1/2), where ERK1/2 increases its own nuclear translocation (Shindo et al., 2016). Therefore, we implemented this additional reaction in the model, which led to onset kinetics that matched better the sigmoidicity of cortical and striatal data (compare Fig. 6B with Fig. 2). This reaction scheme for dynamic translocation rate was included in the model for all further simulations.

Striatal neurons exhibit higher levels of PKA than cortical neurons, in particular the RIIβ type (Brandon et al., 1998; Cadd and McKnight, 1989; Ilouz et al., 2017; Ventra et al., 1996), which we also see in our brain slice preparations from young mice (Fig. S1). We tested whether this difference in PKA level could be a contributing factor to the observed differences between the cortical and striatal nuclear response, and we ran simulations with various initial amounts of PKA. As expected, reducing the PKA levels decreased the nuclear response amplitude (Fig. 6C). A significant reduction in PKA levels (0.2×) almost fully suppressed the nuclear response towards transient dopamine input, similar to what was observed in the cortex (Fig. 6C). Simulation in that low PKA condition with reduced PDE did not significantly increase the

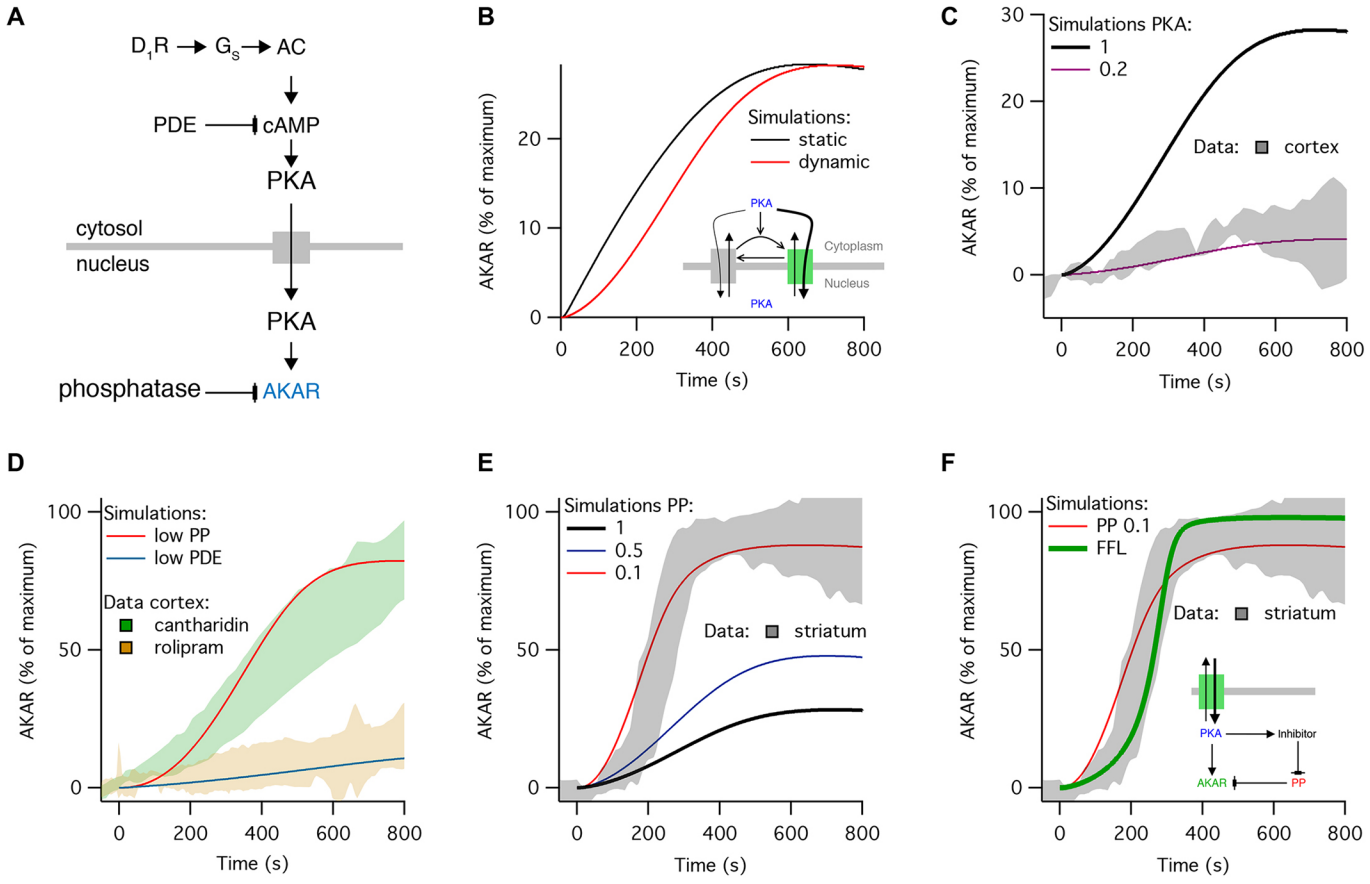

Fig. 6. Computational modeling indicates a PKA-mediated facilitation of nuclear translocation in cortex and striatum, and a positive feed-forward loop in striatal neurons. (A) Modeled signaling pathway for the dopamine-induced AKAR response in the nucleus. (B–F) Simulated AKAR (lines) and measured AKAR2-NLS (gray and colored shaded areas represent mean±s.e.m). (B) Modeling the translocation reaction with a single-static translocation rate (black) or a dynamic translocation rate with PKA increasing its own translocation by phosphorylation of the nuclear pore (red; reaction schematic in inset). All further simulations assume this condition. (C) Simulation of nuclear AKAR response with PKA levels 1× (black) and 0.2× (purple); response to 10 s SKF measured in the cortex. (D) Simulation of nuclear AKAR response with low PKA (0.2×) with low protein phosphatase (PP, red) or low PDE (blue); responses to 10 s SKF measured in the cortex with cantharidin (green shade) and rolipram (orange shade). (E) Dopamine input with 1× PKA and various protein phosphatases levels (1×, 0.5× and 0.1×); the response to 10 s SKF measured in the striatum. (F) Simulation of nuclear AKAR response (green trace) with a PKA-dependent protein phosphatase inhibition feedforward loop (FFL) in the nucleus (inset) and 1× protein phosphatase level. The red trace is a copy of the red trace in E shown for comparison.

Journal of Cell Science (2018) 131, jcs216556. doi:10.1242/jcs.216556

nuclear response (Fig. 6D), consistent with our measures in cortical neurons in the presence of PDE inhibitor (Fig. 5D). On the other hand, suppressing the activity of protein phosphatases in the same condition led to a large nuclear response (Fig. 6D), which looked similar to the cortical responses measured in the presence of protein phosphatases inhibitor (Fig. 5F). The low cytosolic PKA condition of the model thus seems to recapitulate the observations made for the neurons of the prefrontal cortex, suggesting that PKA is a limiting resource responsible for the low nuclear responsiveness in these neurons.

On the other hand, even though the default (1×) PKA level in the cytosol was validated by the cytosolic responses measured in the striatum (Yapo et al., 2017), the simulation output of the model did not match the large amplitude of the observed nuclear responses (Fig. 6C, compare with Fig. 2A). This could be due to the dephosphorylation activity of protein phosphatases (protein phosphatases) in the nucleus, which counteracts PKA-dependent phosphorylation. Thus, we ran simulations with decreasing levels of nuclear protein phosphatases, while keeping the default (1×) PKA level. A 10-fold reduction in protein phosphatases level increased the nuclear response amplitude to a level that matched the amplitude of the response to transient dopamine stimulation (Fig. 6E).

Even though these simulations suggest that very low level of nuclear protein phosphatases is required to reproduce the striatal response, such a low level is inconsistent with the previous report that protein phosphatases are abundantly localized in the nucleus of MSNs (Ouimet et al., 1995). However, striatal MSNs express multiple regulatory proteins, such as DARPP-32 and Inhibitor-1 (PPP1R1A), that form a feed-forward loop (FFL) to transiently suppress protein phosphatase activity in a PKA-dependent fashion: these regulatory proteins are phosphorylated by PKA and thus become potent inhibitors of protein phosphatases (Walaas et al., 2011). With the striatal default protein phosphatase activity (1×) together with this FFL introduced into the nuclear compartment (Fig. 6F, inset), the model produced a nuclear response that was similar to the measured striatal data (Fig. 6F). Furthermore, the kinetic profile of the simulated response with FFL had a closer resemblance with the measured striatal data than the simulated response at low protein phosphatases condition (Fig. 6F). Thus, even though the striatal nucleus may contain high levels of protein phosphatases, a PKA-dependent protein phosphatase inhibition mechanism could produce a time window of temporarily low protein phosphatase activity during which PKA signaling dominates, which could be a possible explanation for the higher sensitivity of the striatal nuclear response. Such an FFL mechanism may also contribute to the sharp transition from a lack of response to maximal response with only a small increment in cAMP signal, thus producing the off-on switch that we observed in the striatum (Fig. 3).

Taken together, these simulations support the hypothesis that the balance of PKA and protein phosphatase activities could strongly affect the nuclear integration of neuromodulatory signals in neurons, and explain the differences we observed between cortical and striatal nuclear response (Fig. 7A,B). A condition with a low level of PKA that is unable to counteract the nuclear protein phosphatase activity explains the diminished responsiveness of the cortical neurons. By contrast, higher PKA activity together with low protein phosphatase activity, possibly via PKA-dependent protein phosphatase inhibition in the nuclear compartment, could lead to highly sensitive nuclear responses, as observed in the striatum.

DISCUSSION

Signal transduction from the membrane to the nuclear compartment plays a pivotal role in neuronal adaptations associated with long-lasting changes in gene expression (Cohen and Greenberg, 2008; Matamales and Girault, 2011). Our data obtained from biosensor imaging in brain slices reveal that the dynamics of signal transduction in striatal neurons differ profoundly from those in other cell types, including cortical neurons, with PKA producing fast phosphorylations in the nuclear compartment, in an all-or-none manner. Taken together with computer modeling, our results suggest that this unique striatal feature results from a high PKA to protein phosphatase activity ratio, strongly regulated by a positive feed-forward mechanism.

Nuclear PKA activity usually reflects the cytosolic PKA signal, which is progressively dampened in amplitude and kinetics as it propagates from the membrane through the cytosol and into the nucleus. This has been reported in various cell types (DiPilato et al., 2004; Haj Slimane et al., 2014; Sample et al., 2012; Yang et al., 2014). Neuronal cells provide an additional level of complexity, with cAMP–PKA signals being confined in specific subcellular

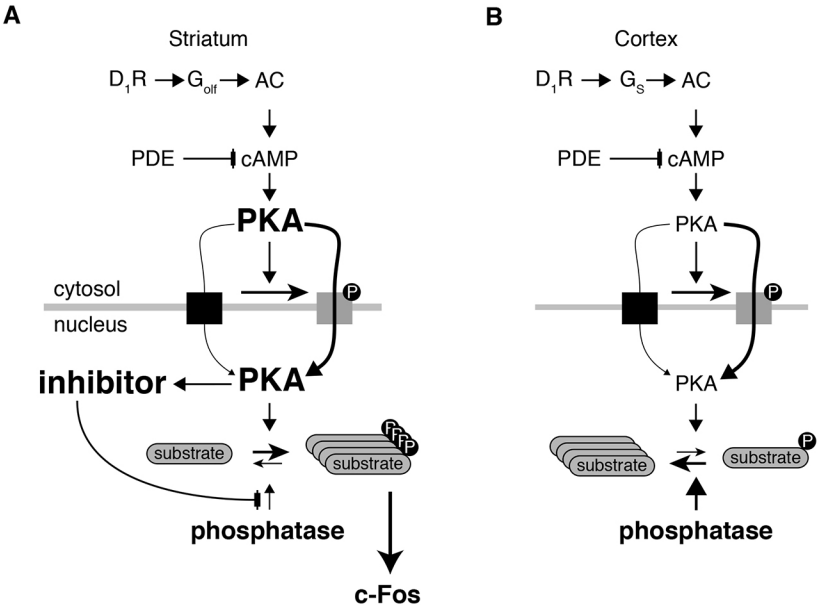

Fig. 7. High PKA level and tight regulation of nuclear phosphatase activity increase responsiveness of striatal neurons to transient dopamine. Transient dopamine input increases cAMP levels and activates cytoplasmic PKA in the striatum (A) and cortex (B). PKA passively diffuses into the nucleus through the nuclear pore. The sigmoidal increase in substrate phosphorylation in the nucleus suggests that PKA activity increases the permeability of the nuclear pore, possibly via phosphorylation. In the cortex, the balance between low PKA level and high phosphatase activity leads to little phosphorylation of intranuclear substrates. In the striatum, a high level of PKA together with a positive feedforward loop involving a phosphatase inhibitor (probably DARPP-32) results in the efficient phosphorylation of nuclear PKA substrates. These specificities of striatal neurons may account for the non-linear integration of PKA signal in the nucleus, allowing for the transduction of transient dopamine signals associated with reward into c-Fos expression.

Journal of Cell Science (2018) 131, jcs216556. doi:10.1242/jcs.216556

domains, such as dendrites and axon terminals without affecting other cellular domains (Calebiro and Maiellaro, 2014; Gervasi et al., 2010; Maiellaro et al., 2016). However, signal translocation from the somatic cytosol to the nucleus in neurons seems to follow the general rule of a slow diffusion, as observed in cortical and thalamic neurons with neuropeptide or 5-HT_7 receptor stimulation (Gervasi et al., 2007; Hu et al., 2011). Our observations here on cortical neurons are consistent with this theory, showing a slow and gradual nuclear PKA response to D_1 receptor stimulation. Striatal neurons strikingly depart from this classical scheme, with a large PKA signal in the nucleus triggered by correspondingly modest cytosolic responses (Fig. 1). The kinetics of this signal in striatal neurons also differs from the slow integration observed in all other cell types, with a minute increase over ∼200 s after receptor stimulation followed by an abrupt rise that reaches the maximal phosphorylation level of the AKAR biosensor in the nucleus. This peculiar temporal profile is observed for all stimulation modalities tested (i.e. stimulation of dopamine D_1 and adenosine A_{2A} receptors, forskolin treatment and cAMP uncaging), showing that this feature is an intrinsic property of cyto-nuclear signal integration and is independent of the origin of the signal. The non-linearity of the nuclear response in the striatum is further illustrated by the switch-like nuclear signal, going abruptly from a lack of response to a maximal response. Again, this lack of intermediate responses was observed with all stimuli and best characterized for very low doses with the D_1 receptor agonist SKF, and contrasted with the wide amplitude spread observed in cortical and other neurons in response to D_1, neuropeptide or 5-HT_7 receptor stimulation (Gervasi et al., 2007; Hu et al., 2011). The transduction of cAMP signals from the dendritic arborization into the nucleus of striatal neurons has already been shown to follow a complex non-monotonic dependency as the distance to the cell body increases (Li et al., 2015). In addition, we have previously reported that, compared to cortical neurons, striatal neurons possessed a signaling machinery endowing them with the ability to strongly respond at the cytosolic level to a brief dopamine signal (Castro et al., 2013; Yapo et al., 2017). In this study, we further reveal another level of integration that boosts the nuclear response to dopamine, again highlighting these striatal neurons as specifically geared to respond to small and/or brief neuromodulatory signals.

Our experiments and computer model simulations highlight the importance of PKA and protein phosphatase activities in determining the net result of PKA action in the nucleus. Low PKA together with tonic protein phosphatase activity prevents nuclear responses in the cortex whereas high levels of PKA and protein phosphatases, together with a positive feed-forward control inhibiting protein phosphatase activity, best matched our observations in the striatum. This model is supported by previous studies showing that the striatum expresses higher levels of PKA compared to the cortex and other brain regions (Brandon et al., 1998; Ventra et al., 1996), as well as by our immunohistochemistry experiments (Fig. S1).

The level of PP1α is also high in MSNs, and particularly in the nucleus (Ouimet et al., 1995). In order to generate an efficient nuclear response, this high level of PP1 must be efficiently inhibited in a PKA-dependent way. DARPP-32 is the natural candidate mediator of this FFL because it powerfully inhibits PP1 (Fienberg et al., 1998; Girault et al., 2017; Hemmings et al., 1984; Svenningsson et al., 2004). Previously, we have observed that the striatal neurons displayed fast, large and long-lasting cytosolic cAMP–PKA responses to transient dopamine stimulation. Inhibition of the PP1-inhibitory activity through a cytosolic FFL exerted by DARPP-32 protein strongly contributed to the sensitivity of the striatal response (Castro et al., 2013). Moreover, DARPP-32 can convey information from the cytoplasm to the nucleus, where it contributes to the amplification of drug-induced gene expression through PP1 inhibition (Stipanovich et al., 2008). Further work is needed to clearly demonstrate the contribution of DARPP-32 in the switch-like function described here. Taken together, a high PKA and phosphatase level together with a phosphatase inhibitor like DARPP-32 form a positive FFL, which can produce delayed responses with fast onset and all-or-none responsiveness.

Regulatory PKA subunits have been reported to be localized in the nucleus, such as RIβ in the nucleus of cerebellar Purkinje neurons or hippocampal interneurons (Ilouz et al., 2017) and such ‘pre-positioning’ of PKA holoenzyme in the nucleus might speed up the transduction of the cytosolic cAMP signal into a nuclear response. However, the delayed nuclear response that we observed in striatal neurons does not fit with this hypothesis, since cAMP diffuses quickly through the nuclear pore (Sample et al., 2012) and should therefore have induced an instantaneous nuclear signal. Moreover, in another set of our experiments, photorelease of cAMP throughout the cell (the nucleus included) triggered nuclear responses that still displayed the same delayed onset. This indicates that the presence of PKA holoenzyme in the nucleus is an unlikely explanation for the fast and sensitive responsiveness of MSN nuclei. PKA however needs to be located close to the nucleus, and the RIIβ type, which is the dominant type of PKA in both cortical and striatal neurons, favors the translocation of the signal into the nucleus (Cassano et al., 1996; Paolillo et al., 1999). Tethering of regulatory subunits on A kinase-anchoring proteins (AKAPs) in the cell body has also been shown to play a role in the amplification of the PKA signal in the nucleus (Cassano et al., 1996; Dodge-Kafka and Kapiloff, 2006; Feliciello et al., 1997; Friedrich et al., 2010; Paolillo et al., 1999).

Our combined experimental and modeling approach also highlighted another so-far overlooked property of cyto-nuclear signal transduction. If the translocation of PKA from the cytosol to the nucleus only depended on passive diffusion, signal onset in the nucleus would be expected to display an exponential shape, whereas biosensor measurements with AKAR2-NLS actually reported a sigmoidal shape. We found in our simulations that a possible way to achieve this sigmoidal kinetic profile is if PKA activation facilitates the translocation of its own catalytic subunits into the nucleus. While phosphorylation is widely known to affect active nuclear transport (Christie et al., 2016), passive diffusion has also been suggested to be regulated by PKA (Mishra and Parnaik, 1995) and ERK1/2 (Shindo et al., 2016). Our data fit with this latter hypothesis and suggest that the regulation of passive diffusion may play a more important role than anticipated.

Overall, our observations are consistent with signal transduction from the cytosol to the nucleus being limited by the passive diffusion of PKA through the nuclear pore, as reported in a number of cellular systems (Gervasi et al., 2007; Haj Slimane et al., 2014; Harootunian et al., 1993; Martin et al., 2007; Meinkoth et al., 1990; Sample et al., 2012; Yang et al., 2014), with a facilitation of pore diffusion mediated by PKA. Striatal neurons obey to this mechanism, but also feature an additional positive FFL, which provides them with very unusual non-linear properties and a switch-like behavior. We hypothesize that this feature plays an important role in the detection of changes in the extracellular levels of dopamine. The dopamine signals received by striatal neurons cover a wide range of patterns such as tonic release, phasic burst associated with a rewarding event and up to long and sustained

Journal of Cell Science (2018) 131, jcs216556. doi:10.1242/jcs.216556

dopamine levels, such as those produced by addictive drugs (Hart et al., 2014; Heien et al., 2005; Howe et al., 2013). With their high sensitivity and all-or-none responsiveness, the nucleus of MSNs can threshold incoming signals, rejecting fast fluctuations of background dopamine level and brief transients, but responding powerfully to dopamine signals lasting for tens to a few hundred seconds. This mechanism may be required for reward-mediated learning, a condition where the detection of moderately long dopamine transients is a critical requirement. This specific striatal feature may also play a critical role in pathology, when abnormal dopamine signals occur, such as those elicited by addictive drugs, as well as with L-DOPA treatment in Parkinson's disease; such signals activate nuclear targets selectively in striatal neurons and might be responsible for the development of drug-seeking behaviors or dyskinesia (Cerovic et al., 2013; Girault, 2012). Striatal neurons are equipped with a number of unusual signaling proteins such as $G_{\alpha olf}$, AC5, PDE10, DARPP-32, and end-up featuring an edge-detector filter that binarizes dopamine transitions through non-linear integration, in sharp contrast with cortical neurons, which rather appear as linear integrators of a variety of different neuromodulatory signals, with gradual cytosolic and nuclear responses.

MATERIALS AND METHODS

Brain slice preparation

Wild-type C57Bl/6J mice were obtained from Janvier (Le Genest Saint Isle, France). Mice were maintained in a 12 h light–12 h dark cycle, in stable conditions of temperature (22°C), with food and water available *ad libitum*. All the experiments were performed according to French Ministry of Agriculture and Forestry guidelines for handling animals (decree 87-848).

Brain slices from male mice aged from 7 to 11 days were prepared as previously described (Castro et al., 2010). Briefly, mice were killed by decapitation and the brain was quickly removed. Coronal and sagittal brain slices were cut with a VT1200S microtome (Leica, Germany). Slices were prepared in an ice-cold solution of the following composition: 125 mM NaCl, 0.4 mM $CaCl_2$, 1 mM $MgCl_2$, 1.25 mM NaH_2PO_4, 26 mM $NaHCO_3$, 5 mM sodium pyruvate, 20 mM glucose and 1 mM kynurenic acid, saturated with 5% CO_2 and 95% O_2. The slices were incubated in this solution for 30 min and then placed on a Millicell-CM membrane (Millipore) in culture medium (50% Minimum Essential Medium, 50% Hanks' Balanced Salt Solution, 6.5 g/l glucose, penicillin-streptomycin, Invitrogen). We used the Sindbis virus as a vector to induce expression of the biosensors after overnight incubation (Ehrengruber et al., 1999). The coding sequences of AKAR3 (Allen and Zhang, 2006) and AKAR2-NLS (Zhang et al., 2005) were inserted into the viral vector pSinRep5 (Invitrogen, San Diego, CA), as previously described (Gervasi et al., 2007). Viral particles (~5×10^5 particles per slice) were added and slices were incubated overnight at 35°C under an atmosphere containing 5% CO_2. Before the experiment, slices were incubated for 30 min in the recording solution (identical to the solution used for cutting, except that the Ca^{2+} concentration was 2 mM and kynurenic acid was omitted). During recordings, brain slices were continuously perfused with this solution saturated with 5% CO_2 and 95% O_2, at 32°C. Most drugs applied on the slices were added in this continuous bath perfusion.

The viability of the neurons in these experimental conditions have been checked by patch-clamp recording, which showed electrical activity to be normal (Castro et al., 2010; Gervasi et al., 2007).

Optical recordings on brain slices

Recordings were made on visually identified medium-sized spiny neurons (MSNs) in the striatum or pyramidal neurons in layer V of the prefrontal cortex (lateral +1.1 mm to 1.56 mm; bregma +1.8 mm to 2.2 mm). In the striatum, neurons were selected for a diameter less than 13 µm, comparable to the size known for MSNs, which constitute 95% of the neurons in the striatum. Larger neurons, presumably cholinergic interneurons, were excluded from analysis. In all recordings, we confirmed the presence of D_1 receptors on the imaged neurons with a pharmacological challenge at the end of the recording with the D_1-like agonist SKF-38393. Wide-field images were obtained with an Olympus BX50WI or BX51WI upright microscope with a 20×0.5 NA or a 40×0.8 NA water-immersion objective, and an ORCA-AG camera (Hamamatsu). Images were acquired with iVision software (Biovision, Exton, PA). The excitation and dichroic filters were D436/20 and 455dcxt. Signals were acquired by alternating the emission filters, HQ480/40 for the donor and D535/40 for the acceptor, with a filter wheel (Sutter Instruments, Novato, CA). All filters were obtained from Chroma Technology (Brattleboro, VT, USA).

Images were analyzed with custom routines written in the IGOR Pro 7 environment (Wavemetrics, Lake Oswego, OR, USA) following the algorithm previously described (Polito et al., 2014). The emission ratio was calculated for each pixel for the ratio of florescence at 535 nm to that at 480 nm (F535/F480) for both AKAR biosensors. The pseudocolor images were calculated so as to display the ratio value coded in hue and the fluorescence of the preparation coded in intensity. A calibration square indicates the intensity values from left to right and the ratio values from bottom to top. The size of the square indicates the scale of the image in microns. No correction for bleed-through or direct excitation of the acceptor was applied because we considered the correction coefficients to be potentially unreliable in the brain slice preparations due to differences in optical properties between slices. Bleed-through and direct excitation corrections increase the apparent ratio changes but without improving signal-to-noise ratio (Ducros et al., 2009). The ratio changes in our conditions therefore appear smaller than those reported by other studies in which such corrections were applied.

Dopamine uncaging and fast drug application

Photorelease of dopamine from NPEC-DA was performed using a 360 nm LED source mounted on the epifluorescence port of the microscope, providing 0.7 mW at the exit of the 40× microscope objective (UVILED, Rapp OptoElectronic, Hamburg, Germany). The UV flash triggers the instantaneous release of free dopamine, which concentration declines with a time-constant of 109 s, as previously described (Yapo et al., 2017). The frequency of data acquisition, usually 1 image pair every 50 s, was increased to 1 pair every 5 s, starting ten data points before dopamine uncaging.

A fast focal application system was used for kinetic studies (Gervasi et al., 2007). A glass pipette (80–120 µm tip diameter) was placed 300 µm to the side of and 200 µm above the brain slice, and ejected the drug contained in the same solution as the bath. The same device was used for the sustained or transient (10 s) application of 1 µM SKF-38393, 1 µM CGS 21680 or 13 µM forskolin+200 µM IBMX. The frequency of data acquisition during the fast drug application was set to 1 pair every 10 s.

Immunohistochemistry

We carried out c-Fos immunohistochemistry with a standard peroxidase-based method (Vectastain Elite ABC Kit, Vector Laboratories, UK), using 3,3′-diaminobenzidine (Sigma-Aldrich) as the chromogenic substrate. The primary c-Fos antiserum was used at a dilution of 1:1000 (rabbit polyclonal antiserum from Santa Cruz Biotechnology). Before immunohistochemistry, brain slices were stimulated with dopamine which was released either by local flash photolysis of NPEC-dopamine (0.1 s or 1 s, in the cortex or striatum) or bath application of forskolin (13 µM, 5 min) in the recording solution. After stimulation and incubation for 90 min at 32°C, brain slices were fixed by overnight immersion in phosphate-buffered 4% paraformaldehyde at 4°C, pH 7.4. Slices were then rinsed three times in ice-cold phosphate buffer and incubated with an avidin-biotin blocking kit. Positive nuclei were counted by a researcher blind to the experimental conditions, with a 20× water-immersion objective, on four adjacent regions of 1400 μm^2 each, on at least three slices per condition. Immunostaining of the PKA regulatory subunit RIIβ was performed in brain slices fixed by overnight immersion in phosphate-buffered 4% paraformaldehyde at 4°C, pH 7.4. Slices were then rinsed three times in ice-cold phosphate buffer containing 2% goat serum, 1% BSA and 0.2% Triton X-100). The primary anti-RIIβ antibody (BD Transduction Laboratories; cat. no. 610625; 1:500 dilution) was incubated overnight at 4°C. Slices were rinsed and incubated with a secondary antibody (Alexa Fluor 488 goat anti-mouse IgG, ThermoFisher; diluted 1:500) for 2 h at room temperature. As a negative control, the secondary antibody applied

alone (without the primary antibody step) showed no reactivity. Images were acquired with wide-field imaging.

Data analysis

The FRET change in the AKAR3 and AKAR2-NLS biosensors was quantified by ratiometric imaging, with PKA-dependent phosphorylation inducing an increase in the acceptor:donor ratio. The measured acceptor:donor ratio fluctuates between the R_{min} and R_{max} values, which correspond to the minimal ratio value (no biological signal) and maximal response (saturated biosensor) (Grynkiewicz et al., 1985). The maximal response corresponding to biosensor saturation was determined for each neuron at the end of the recording. This level was determined by applying 13 µM forskolin, sufficient to maximally phosphorylate the highly sensitive probe AKAR3 (Gervasi et al., 2007). The baseline ratio was considered to be close to R_{min}, as shown previously (Polito et al., 2015). Absolute ratio values differed between cells, so the amplitude of the response to receptor stimulation was quantified for each neuron as the fractional change in ratio from its own baseline and maximal final ratio response. In wide-field imaging experiments, some of the signal measured on a region of interest comes from out-of-focus neurons. This has no effect on the kinetics features of the ratio signal, but affects the absolute amplitude of the response when out-of-focus neurons have a pharmacological response different from that of the in-focus neuron. Still, for a given region of interest, the steady-state response to a bath-applied saturating dose (1 µM) of SKF-38393 was genuinely representative of the response of all D_1-expressing neurons contributing to the signal of this region of interest, and this value was used for normalization in kinetic analyses.

Drugs

NPEC-caged dopamine [(N)-1-(2-nitrophenyl) ethylcarboxy-3, 4-dihydroxyphenethylamine], SKF-38393 hydrobromide, CGS 21680 hydrochloride, rolipram, cantharidin, cyclosporin A, FK 506, fostriecin, and forskolin (fsk) were obtained from Tocris Cookson (Bristol, UK); 3-isobutyl-1-methylxanthine (IBMX) was obtained from Sigma-Aldrich. DMNB-cAMP (4,5-dimethoxy-2-nitrobenzyl adenosine 3,5′-cyclic monophosphate) was from Molecular Probes.

Computational modeling

The signaling cascade related to the D_1-dependent activation of PKA and its nuclear translocation was modeled as a system of biochemical reactions which contains both reversible and irreversible reactions. Enzymatic reactions were represented as a two-step process in which the first step is a reversible binding between the enzyme and substrate, and the second step is an irreversible transformation of the enzyme-substrate complex into product and thereby releasing free enzyme. Individual reactions were mathematically modeled as ordinary differential equations (ODEs) corresponding to the rate law of mass action kinetics as described previously (Yapo et al., 2017).

The resulting system of ODEs was numerically solved using ode15 s solver provided in the Simbiology toolbox of MATLAB (MathWorks) with a maximum timestep of 0.01 s. Explicit spatial or geometrical aspects were not taken into account in the model. However, the whole signaling volume was divided into two abstract subvolumes or compartments representing cytosol and nucleus and they contain cytosolic and nuclear reactions, respectively. The total volume of the whole reaction space assumed in the model is around 550 µm^3, which contains a nuclear volume of ∼400 µm^3, resulting in a cytoplasmic volume of around ∼150 µm^3. The cytosolic volume contains the chemical reactions related to D_1-dependent PKA activation. Briefly, dopamine-dependent D_1 activation leads to an increase in GTP-bound stimulatory G-protein, which in turn activates adenylyl cyclase (AC). AC activation results in the elevation of cAMP, which in turn activates PKA. The cytosolic compartment also contains PDE to degrade cAMP. Active PKA translocates to the nuclear compartment where it could phosphorylate AKAR present in this compartment. The nuclear compartment also contains protein phosphatases which could dephosphorylate AKAR. The intercompartmental PKA translocation is implemented as a first-order reaction. Alternatively, a dynamic forward kinetic rate is used for this reaction to capture the sigmoidal nature of nuclear signal observed in the current data. This dynamic forward reaction rate for cyto-nuclear PKA translocation assumes that it is positively influenced by the level of active PKA in the cytoplasmic compartment. This PKA dependency is implemented using a chemical species corresponding to a nuclear channel that is phosphorylated by PKA, and the overall forward reaction rate is calculated at each simulation timestep by averaging a low reaction rate weighted by the fraction of the non-phosphorylated form and a high reaction rate weighted by the fraction of the phosphorylated form of the nuclear channel species. An additional PKA-dependent protein phosphatase inhibition reaction scheme in the nuclear compartment was also tested. Biochemical reactions and respective parameters for all these processes in the cytosolic and nuclear compartments, except the PKA translocation and PKA-dependent PP1 inhibition, are directly taken from the recently published reaction-kinetic model of dopamine-dependent cAMP signaling (Yapo et al., 2017). In all the simulations, D_1 receptor is activated with a transient dopamine input that mimics the fast application of saturating level of SKF-38393 in our experimental protocol (10 s SKF-38393 application). This time-varying input is modeled as an instantaneous increase in dopamine to 10 µM followed by an exponential decay with a time constant of ∼150 s, which reflects the diffusion rate of the drug out of the brain slice (Yapo et al., 2017).

Statistics

At least four neurons were analyzed per brain slice and their responses averaged. '*N*' indicates the number of independent experiments (i.e. brain slices), and '*n*' indicates the number of cells. Data are expressed as mean±s.e.m. Differences were considered significant when $P<0.05$. The probability density (Fig. 3) was estimated using a Gaussian kernel and Silverman's bandwidth selection in Igor Pro 7 (Wavemetrics).

Acknowledgements

We want to thank Mohamed Doulazmi for performing statistical tests. The group of C.Y., P.V. and L.R.V.C. is member of the Bio-Psy Labex.

Competing interests

The authors declare no competing or financial interests.

Author contributions

Conceptualization: C.Y., A.G.N., P.V., L.R.V.C.; Methodology: A.G.N., P.V., L.R.V.C.; Software: A.G.N., P.V.; Validation: C.Y., A.G.N., P.V., L.R.V.C.; Formal analysis: C.Y., A.G.N.; Investigation: C.Y., L.R.V.C.; Data curation: P.V., L.R.V.C.; Writing - original draft: C.Y., A.G.N., P.V., L.R.V.C.; Writing - review & editing: C.Y., A.G.N., P.V., L.R.V.C.; Visualization: C.Y., P.V., L.R.V.C.; Supervision: J.H.K., P.V., L.R.V.C.; Project administration: P.V.; Funding acquisition: J.H.K., P.V.

Funding

This work was funded by 'DIM Cerveau et Pensée IdF 2014', the Association France Parkinson, the European Horizon 2020 Framework Program under grant agreement no. 720270 (Human Brain Project SGA1) and EuroSPIN – an Erasmus Mundus Joint Doctoral program. This work was supported by the Investissements d'Avenir program managed by the Agence Nationale de la Recherche (ANR) under reference ANR-11-IDEX-0004-02.

Supplementary information

Supplementary information available online at
http://jcs.biologists.org/lookup/doi/10.1242/jcs.216556.supplemental

References

Allen, M. D. and Zhang, J. (2006). Subcellular dynamics of protein kinase A activity visualized by FRET-based reporters. *Biochem. Biophys. Res. Commun.* **348**, 716-721.

Arbuthnott, G. W. and Wickens, J. (2007). Space, time and dopamine. *Trends Neurosci.* **30**, 62-69.

Beaulieu, J.-M., Espinoza, S. and Gainetdinov, R. R. (2015). Dopamine receptors-IUPHAR Review 13. *Br. J. Pharmacol.* **172**, 1-23.

Brandon, E. P., Logue, S. F., Adams, M. R., Qi, M., Sullivan, S. P., Matsumoto, A. M., Dorsa, D. M., Wehner, J. M., Mcknight, G. S. and Idzerda, R. L. (1998). Defective motor behavior and neural gene expression in RIIbeta-protein kinase A mutant mice. *J. Neurosci.* **18**, 3639-3649.

Bromberg-Martin, E. S., Matsumoto, M. and Hikosaka, O. (2010). Dopamine in motivational control: rewarding, aversive, and alerting. *Neuron* **68**, 815-834.

Cadd, G. and Mcknight, G. S. (1989). Distinct patterns of cAMP-dependent protein kinase gene expression in mouse brain. *Neuron* **3**, 71-79.

Calebiro, D. and Maiellaro, I. (2014). cAMP signaling microdomains and their observation by optical methods. *Front. Cell Neurosci.* **8**, 350.

Cassano, S., Gallo, A., Buccigrossi, V., Porcellini, A., Cerillo, R., Gottesman, M. E. and Avvedimento, E. V. (1996). Membrane localization of cAMP-dependent protein kinase amplifies cAMP signaling to the nucleus in PC12 cells. *J. Biol. Chem.* **271**, 29870-29875.

Castro, L. R. V., Gervasi, N., Guiot, E., Cavellini, L., Nikolaev, V. O., Paupardin-Tritsch, D. and Vincent, P. (2010). Type 4 phosphodiesterase plays different integrating roles in different cellular domains in pyramidal cortical neurons. *J. Neurosci.* **30**, 6143-6151.

Castro, L. R. V., Brito, M., Guiot, E., Polito, M., Korn, C. W., Hervé, D., Girault, J.-A., Paupardin-Tritsch, D. and Vincent, P. (2013). Striatal neurones have a specific ability to respond to phasic dopamine release. *J. Physiol.* **591**, 3197-3214.

Cerovic, M., D'isa, R., Tonini, R. and Brambilla, R. (2013). Molecular and cellular mechanisms of dopamine-mediated behavioral plasticity in the striatum. *Neurobiol. Learn. Mem.* **105**, 63-80.

Chergui, K., Nomikos, G. G., Mathé, J. M., Gonon, F. and Svensson, T. H. (1996). Burst stimulation of the medial forebrain bundle selectively increase Fos-like immunoreactivity in the limbic forebrain of the rat. *Neuroscience* **72**, 141-156.

Christie, M., Chang, C.-W., Róna, G., Smith, K. M., Stewart, A. G., Takeda, A. A. S., Fontes, M. R. M., Stewart, M., Vértessy, B. G., Forwood, J. K. et al. (2016). Structural biology and regulation of protein import into the nucleus. *J. Mol. Biol.* **428**, 2060-2090.

Cohen, S. and Greenberg, M. E. (2008). Communication between the synapse and the nucleus in neuronal development, plasticity, and disease. *Annu. Rev. Cell Dev. Biol.* **24**, 183-209.

Dipilato, L. M., Cheng, X. and Zhang, J. (2004). Fluorescent indicators of cAMP and Epac activation reveal differential dynamics of cAMP signaling within discrete subcellular compartments. *Proc. Natl. Acad. Sci. USA* **101**, 16513-16518.

Dodge-Kafka, K. L. and Kapiloff, M. S. (2006). The mAKAP signaling complex: integration of cAMP, calcium, and MAP kinase signaling pathways. *Eur. J. Cell Biol.* **85**, 593-602.

Ducros, M., Moreaux, L., Bradley, J., Tiret, P., Griesbeck, O. and Charpak, S. (2009). Spectral unmixing: analysis of performance in the olfactory bulb in vivo. *PLoS ONE* **4**, e4418.

Ehrengruber, M. U., Lundstrom, K., Schweitzer, C., Heuss, C., Schlesinger, S. and Gähwiler, B. H. (1999). Recombinant Semliki Forest virus and Sindbis virus efficiently infect neurons in hippocampal slice cultures. *Proc. Natl. Acad. Sci. USA* **96**, 7041-7046.

Feliciello, A., Li, Y., Avvedimento, E. V., Gottesman, M. E. and Rubin, C. S. (1997). A-kinase anchor protein 75 increases the rate and magnitude of cAMP signaling to the nucleus. *Curr. Biol.* **7**, 1011-1014.

Fienberg, A. A., Hiroi, N., Mermelstein, P. G., Song, W., Snyder, G. L., Nishi, A., Cheramy, A., O'callaghan, J. P., Miller, D. B. and Cole, D. G. (1998). DARPP-32: regulator of the efficacy of dopaminergic neurotransmission. *Science* **281**, 838-842.

Friedrich, M. W., Aramuni, G., Mank, M., Mackinnon, J. A. G. and Griesbeck, O. (2010). Imaging CREB activation in living cells. *J. Biol. Chem.* **285**, 23285-23295.

Gervasi, N., Hepp, R., Tricoire, L., Zhang, J., Lambolez, B., Paupardin-Tritsch, D. and Vincent, P. (2007). Dynamics of protein kinase A signaling at the membrane, in the cytosol, and in the nucleus of neurons in mouse brain slices. *J. Neurosci.* **27**, 2744-2750.

Gervasi, N., Tchénio, P. and Preat, T. (2010). PKA dynamics in a Drosophila learning center: coincidence detection by rutabaga adenylyl cyclase and spatial regulation by dunce phosphodiesterase. *Neuron* **65**, 516-529.

Girault, J.-A. (2012). Signaling in striatal neurons: the phosphoproteins of reward, addiction, and dyskinesia. *Prog. Mol. Biol. Transl. Sci.* **106**, 33-62.

Girault, J.-A., Greengard, P. and Nairn, A. C. (2017). Regulation of striatal signaling by protein phosphatases. In *Handbook of Behavioral Neuroscience: Handbook of Basal Ganglia Structure and Function*, 2nd edn (eds, H. Steiner and K. Y. Tseng), pp. 583-607. Elsevier.

Graybiel, A. M., Moratalla, R. and Robertson, H. A. (1990). Amphetamine and cocaine induce drug-specific activation of the c-fos gene in striosome-matrix compartments and limbic subdivisions of the striatum. *Proc. Natl. Acad. Sci. USA* **87**, 6912-6916.

Grynkiewicz, G., Poenie, M. and Tsien, R. Y. (1985). A new generation of Ca2+ indicators with greatly improved fluorescence properties. *J. Biol. Chem.* **260**, 3440-3450.

Hagiwara, M., Brindle, P., Harootunian, A., Armstrong, R., Rivier, J., Vale, W., Tsien, R. and Montminy, M. R. (1993). Coupling of hormonal stimulation and transcription via the cyclic AMP-responsive factor CREB is rate limited by nuclear entry of protein kinase A. *Mol. Cell. Biol.* **13**, 4852-4859.

Haj Slimane, Z., Bedioune, I., Lechêne, P., Varin, A., Lefebvre, F., Mateo, P., Domergue-Dupont, V., Dewenter, M., Richter, W., Conti, M. et al. (2014). Control of cytoplasmic and nuclear protein kinase A by phosphodiesterases and phosphatases in cardiac myocytes. *Cardiovasc. Res.* **102**, 97-106.

Harlan, R. E. and Garcia, M. M. (1998). Drugs of abuse and immediate-early genes in the forebrain. *Mol. Neurobiol.* **16**, 221-267.

Harootunian, A. T., Adams, S. R., Wen, W., Meinkoth, J. L., Taylor, S. S. and Tsien, R. Y. (1993). Movement of the free catalytic subunit of cAMP-dependent protein kinase into and out of the nucleus can be explained by diffusion. *Mol. Biol. Cell* **4**, 993-1002.

Hart, A. S., Rutledge, R. B., Glimcher, P. W. and Phillips, P. E. M. (2014). Phasic dopamine release in the rat nucleus accumbens symmetrically encodes a reward prediction error term. *J. Neurosci.* **34**, 698-704.

Heien, M. L. A. V., Khan, A. S., Ariansen, J. L., Cheer, J. F., Phillips, P. E. M., Wassum, K. M. and Wightman, R. M. (2005). Real-time measurement of dopamine fluctuations after cocaine in the brain of behaving rats. *Proc. Natl. Acad. Sci. USA* **102**, 10023-10028.

Hemmings, H. C. J., Greengard, P., Tung, H. Y. L. and Cohen, P. (1984). DARPP-32, a dopamine-regulated neuronal phosphoprotein, is a potent inhibitor of protein phosphatase-1. *Nature* **310**, 503-505.

Howard, C. D., Pastuzyn, E. D., Barker-Haliski, M. L., Garris, P. A. and Keefe, K. A. (2013). Phasic-like stimulation of the medial forebrain bundle augments striatal gene expression despite methamphetamine-induced partial dopamine denervation. *J. Neurochem.* **125**, 555-565.

Howe, M. W., Tierney, P. L., Sandberg, S. G., Phillips, P. E. M. and Graybiel, A. M. (2013). Prolonged dopamine signalling in striatum signals proximity and value of distant rewards. *Nature* **500**, 575-579.

Hu, E., Demmou, L., Cauli, B., Gallopin, T., Geoffroy, H., Harris-Warrick, R. M., Paupardin-Tritsch, D., Lambolez, B., Vincent, P. and Hepp, R. (2011). VIP, CRF, and PACAP act at distinct receptors to elicit different cAMP/PKA dynamics in the neocortex. *Cereb. Cortex* **21**, 708-718.

Ilouz, R., Lev-Ram, V., Bushong, E. A., Stiles, T. L., Friedmann-Morvinski, D., Douglas, C., Goldberg, G., Ellisman, M. H. and Taylor, S. S. (2017). Isoform-specific subcellular localization and function of protein kinase A identified by mosaic imaging of mouse brain. *Elife* **6**, e17681.

Kim, M., Park, A. J., Havekes, R., Chay, A., Guercio, L. A., Oliveira, R. F., Abel, T. and Blackwell, K. T. (2011). Colocalization of protein kinase A with adenylyl cyclase enhances protein kinase A activity during induction of long-lasting long-term-potentiation. *PLoS Comput. Biol.* **7**, e1002084.

Le Moine, C. and Bloch, B. (1995). D1 and D2 dopamine receptor gene expression in the rat striatum: sensitive cRNA probes demonstrate prominent segregation of D1 and D2 mRNAs in distinct neuronal populations of the dorsal and ventral striatum. *J. Comp. Neurol.* **355**, 418-426.

Li, L., Gervasi, N. and Girault, J.-A. (2015). Dendritic geometry shapes neuronal cAMP signalling to the nucleus. *Nat. Commun.* **6**, 6319.

Maiellaro, I., Lohse, M. J., Kittel, R. J. and Calebiro, D. (2016). cAMP signals in drosophila motor neurons are confined to single synaptic boutons. *Cell Rep.* **17**, 1238-1246.

Martin, B. R., Deerinck, T. J., Ellisman, M. H., Taylor, S. S. and Tsien, R. Y. (2007). Isoform-specific PKA dynamics revealed by dye-triggered aggregation and DAKAP1alpha-mediated localization in living cells. *Chem. Biol.* **14**, 1031-1042.

Matamales, M. and Girault, J.-A. (2011). Signaling from the cytoplasm to the nucleus in striatal medium-sized spiny neurons. *Front. Neuroanat.* **5**, 37.

Meinkoth, J. L., Ji, Y., Taylor, S. S. and Feramisco, J. R. (1990). Dynamics of the distribution of cyclic AMP-dependent protein kinase in living cells. *Proc. Natl. Acad. Sci. USA* **87**, 9595-9599.

Mishra, K. and Parnaik, V. K. (1995). Essential role of protein phosphorylation in nuclear transport. *Exp. Cell Res.* **216**, 124-134.

Ouimet, C. C., Da Cruz E Silva, E. F. and Greengard, P. (1995). The alpha and gamma 1 isoforms of protein phosphatase 1 are highly and specifically concentrated in dendritic spines. *Proc. Natl. Acad. Sci. USA* **92**, 3396-3400.

Paolillo, M., Feliciello, A., Porcellini, A., Garbi, C., Bifulco, M., Schinelli, S., Ventra, C., Stabile, E., Ricciardelli, G., Schettini, G. et al. (1999). The type and the localization of cAMP-dependent protein kinase regulate transmission of cAMP signals to the nucleus in cortical and cerebellar granule cells. *J. Biol. Chem.* **274**, 6546-6552.

Polito, M., Guiot, E., Gangarossa, G., Longueville, S., Doulazmi, M., Valjent, E., Herve, D., Girault, J.-A., Paupardin-Tritsch, D., Castro, L. R. V. et al. (2015). Selective effects of PDE10A inhibitors on striatopallidal neurons require phosphatase inhibition by DARPP-32. *eNeuro* **2**, 1-15.

Polito, M., Vincent, P. and Guiot, E. (2014). Biosensor imaging in brain slice preparations. *Methods Mol. Biol.* **1071**, 175-194.

Sample, V., Dipilato, L. M., Yang, J. H., Ni, Q., Saucerman, J. J. and Zhang, J. (2012). Regulation of nuclear PKA revealed by spatiotemporal manipulation of cyclic AMP. *Nat. Chem. Biol.* **8**, 375-382.

Schultz, W. (2007). Behavioral dopamine signals. *Trends Neurosci.* **30**, 203-210.

Shindo, Y., Iwamoto, K., Mouri, K., Hibino, K., Tomita, M., Kosako, H., Sako, Y. and Takahashi, K. (2016). Conversion of graded phosphorylation into switch-like nuclear translocation via autoregulatory mechanisms in ERK signalling. *Nat. Commun.* **7**, 10485.

Stipanovich, A., Valjent, E., Matamales, M., Nishi, A., Ahn, J.-H., Maroteaux, M., Bertran-Gonzalez, J., Brami-Cherrier, K., Enslen, H., Corbillé, A.-G. et al. (2008). A phosphatase cascade by which rewarding stimuli control nucleosomal response. *Nature* **453**, 879-884.

Svenningsson, P., Nishi, A., Fisone, G., Girault, J.-A., Nairn, A. C. and Greengard, P. (2004). DARPP-32: an integrator of neurotransmission. *Annu. Rev. Pharmacol. Toxicol.* **44**, 269-296.

Swingle, M. R., Amable, L., Lawhorn, B. G., Buck, S. B., Burke, C. P., Ratti, P., Fischer, K. L., Boger, D. L. and Honkanen, R. E. (2009). Structure-activity relationship studies of fostriecin, cytostatin, and key analogs, with PP1, PP2A, PP5, and (beta12-beta13)-chimeras (PP1/PP2A and PP5/PP2A), provide further insight into the inhibitory actions of fostriecin family inhibitors. *J. Pharmacol. Exp. Ther.* **331**, 45-53.

Threlfell, S. and West, A. R. (2013). Review: modulation of striatal neuron activity by cyclic nucleotide signaling and phosphodiesterase inhibition. *Basal Ganglia.* **3**, 137-146.

Tillo, S. E., Xiong, W.-H., Takahashi, M., Miao, S., Andrade, A. L., Fortin, D. A., Yang, G., Qin, M., Smoody, B. F., Stork, P. J. S. et al. (2017). Liberated PKA catalytic subunits associate with the membrane via myristoylation to preferentially phosphorylate membrane substrates. *Cell Rep.* **19**, 617-629.

Tritsch, N. X. and Sabatini, B. L. (2012). Dopaminergic modulation of synaptic transmission in cortex and striatum. *Neuron* **76**, 33-50.

Valjent, E., Bertran-Gonzalez, J., Hervé, D., Fisone, G. and Girault, J.-A. (2009). Looking BAC at striatal signaling: cell-specific analysis in new transgenic mice. *Trends Neurosci.* **32**, 538-547.

Ventra, C., Porcellini, A., Feliciello, A., Gallo, A., Paolillo, M., Mele, E., Avvedimento, V. E. and Schettini, G. (1996). The differential response of protein kinase A to cyclic AMP in discrete brain areas correlates with the abundance of regulatory subunit II. *J. Neurochem.* **66**, 1752-1761.

Vincent, S. L., Khan, Y. and Benes, F. M. (1993). Cellular distribution of dopamine D1 and D2 receptors in rat medial prefrontal cortex. *J. Neurosci.* **13**, 2551-2564.

Walaas, S. I., Hemmings, H. C. J., Greengard, P. and Nairn, A. C. (2011). Beyond the dopamine receptor: regulation and roles of serine/threonine protein phosphatases. *Front. Neuroanat.* **5**, 50.

Yang, J. H., Polanowska-Grabowska, R. K., Smith, J. S., Shields, C. W. and Saucerman, J. J. (2014). PKA catalytic subunit compartmentation regulates contractile and hypertrophic responses to β-adrenergic signaling. *J. Mol. Cell. Cardiol.* **66**, 83-93.

Yapo, C., Nair, A. G., Clement, L., Castro, L. R., Hellgren Kotaleski, J. and Vincent, P. (2017). Detection of phasic dopamine by D1 and D2 striatal medium spiny neurons. *J. Physiol.* **595**, 7451-7475.

Zhang, H. T., Huang, Y., Jin, S. L., Frith, S. A., Suvarna, N., Conti, M. and O'donnell, J. M. (2002). Antidepressant-like profile and reduced sensitivity to rolipram in mice deficient in the PDE4D phosphodiesterase enzyme. *Neuropsychopharmacology* **27**, 587-595.

Zhang, J., Hupfeld, C. J., Taylor, S. S., Olefsky, J. M. and Tsien, R. Y. (2005). Insulin disrupts beta-adrenergic signalling to protein kinase A in adipocytes. *Nature* **437**, 569-573.

Zippin, J. H., Farrell, J., Huron, D., Kamenetsky, M., Hess, K. C., Fischman, D. A., Levin, L. R. and Buck, J. (2004). Bicarbonate-responsive "soluble" adenylyl cyclase defines a nuclear cAMP microdomain. *J. Cell Biol.* **164**, 527-534.

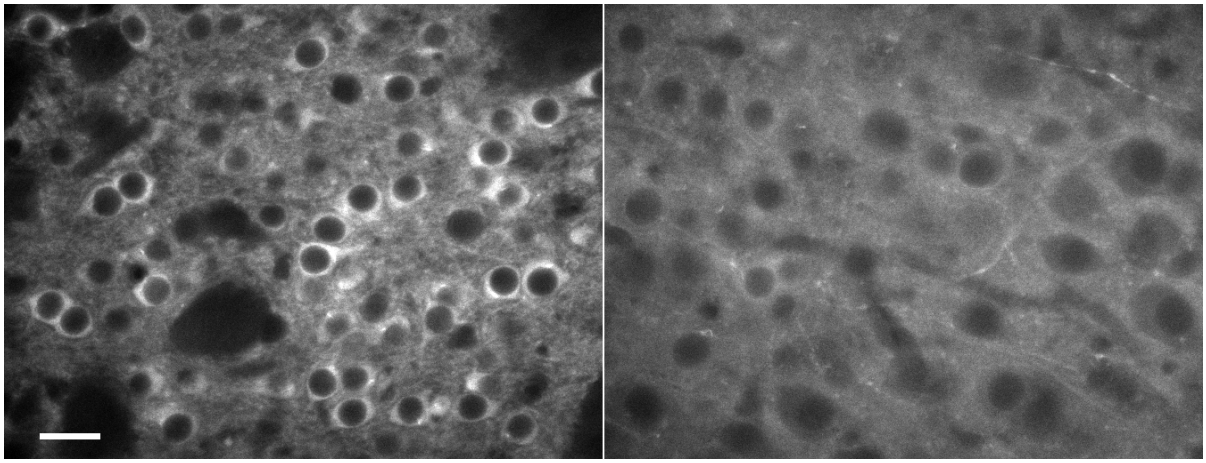

Supplementary Figure 1.
PKA regulatory subunit RIIβ is expressed at a higher level in the soma of striatal neurons than in prefrontal cortex neurons.
Representative images of striatal (left) and cortical (right) brain slices labeled with anti-RIIβ antibodies. Immunostaining shows a high level of RIIβ in striatal neurons, in particular in the somatic cytosol and proximal dendrites. In the cortex, the intensity of the labeling was much lower and mostly localized in dendrites, with a clear reduction in the somatic cytosol. No positive RIIβ staining was observed in the nuclei in both striatum and cortex. The same acquisition and display settings were applied for both images; 40x objective; scale bar: 10 µm; gamma correction: 1.5.